Supporting Information

Linkage Effects of Phenanthrene-based Polymeric Anodes for Lithium-Ion Batteries

Yu-Ruei Kung[a,b,], Huai-Sheng Chin[b], Santosh U. Sharma[c], Li Chen[c], Zi-Yun Ou[c], Hung-Ju Yen[c,*]*

[a] Department of Chemical Engineering and Biotechnology, National Taipei University of Technology, Taipei, Taiwan.

[b] Department of Chemical Engineering and Biotechnology, Tatung University, Taipei, Taiwan

[c] Institute of Chemistry, Academia Sinica, Taipei, Taiwan.

E-mail: yrkung@ntut.edu.tw (Y.-R. Kung); hjyen@gate.sinica.edu.tw (H.-J. Yen)

Supplementary Note 1. Li-ion Battery Cell Preparation and Electrochemical Measurements

The **PQ-polyamides** series polymers were evaluated as anode materials for lithium-ion batteries using a slurry-casting method. The electrode slurry was prepared by thoroughly mixing 40 wt% active polymer material, 50 wt% conductive carbon, and 10 wt% poly(vinylidene fluoride) (PVDF) binder. *N*-Methyl-2-pyrrolidone (NMP) was added as the solvent to obtain a homogeneous slurry. The resulting slurry was uniformly coated onto a copper current collector and initially dried on a hot plate at 60 °C for 12 h, followed by further drying in a vacuum oven at 80 °C for 8 h to ensure complete solvent removal. The dried electrodes were punched into circular disks with a diameter of 12 mm, yielding average active material loadings of approximately 0.17, 0.15, and 0.12 mg cm^{-2}. All electrodes were transferred into an argon-filled glovebox (Vigor, Vigor Tech USA), where the concentrations of oxygen and moisture were maintained below 0.5 ppm. Coin-type half-cells were assembled using the prepared polymer electrodes as the working electrode, lithium metal foil as the counter/reference electrode, and Celgard 2325 as the separator. A total of 40 µL of electrolyte consisting of 1 M $LiPF_6$ dissolved in ethylene carbonate/diethyl carbonate (EC/DEC, 1:1 v/v) was added to each cell.

Electrochemical measurements were carried out using a MultiPalmSens4 electrochemical analyzer (PalmSens BV, Houten, Netherlands) for cyclic voltammetry (CV) tests within a voltage window of 0.02–3.0 V (vs. Li/Li^+). Electrochemical impedance spectroscopy (EIS) measurements were performed at various cycling stages using an electrochemical workstation (Model 7061E, CH Instruments, Inc., Texas, USA) with an applied alternating current (AC) amplitude of 10 mV over a frequency range from 10 mHz to 1 MHz. Galvanostatic charge-discharge cycling was conducted using a programmable battery tester (AcuTech Systems Co. Ltd.) under constant-current mode within the same voltage range of 0.02-3.0 V (vs. Li/Li^+). For each sample, electrochemical measurements were conducted using more than five independent cells ($n > 5$) to ensure the reliability and reproducibility of the data.

Supplementary Note 2. Sweep Rate Voltammetry and Charge-Storage Characteristics

In lithium-ion battery systems, multiple electrochemical processes can occur concurrently within the electrode during cycling. Sweep rate-dependent cyclic voltammetry is a powerful technique for probing these processes and distinguishing their contributions to the overall charge-storage behavior. The total stored charge observed in a CV response can generally be divided into three components[1, 2]:

(i) faradaic charge associated with lithium-ion insertion (diffusion-controlled process), (ii) faradaic charge arising from surface or near-surface redox reactions (pseudocapacitance), and (iii) non-faradaic charge related to electric double-layer capacitance.

In polymer-based electrodes, the contributions from pseudocapacitive and double-layer processes can be significant due to the high surface accessibility and amorphous nature of the electrode materials. The relative contributions of diffusion-controlled and capacitive processes can be evaluated using CV data collected at various scan rates (**Figure S2**). The relationship between the peak current (*i*) and scan rate (*v*) follows the empirical power-law equation:

$$i = av^b$$

where *a* and *b* are adjustable constants. The *b* value is obtained from the slope of the linear fit of $\log i$ versus $\log v$ (**Figure 3c**). A *b* value close to **0.5** indicates a semi-infinite diffusion-controlled process, whereas a value approaching **1.0** suggests a predominantly surface-controlled (capacitive) charge-storage mechanism[3-5]. Since the measured current contains contributions from both diffusion-controlled and capacitive processes, a more detailed separation of these components can be achieved using the following relationship[4, 6, 7]:

$$i = k_1 v + k_2 v^{1/2}$$

where the term $k_1 v$ represents the surface-controlled (capacitive) contribution and $k_2 v^{1/2}$ corresponds to the diffusion-controlled contribution. The values of k_1 and k_2 can be determined by plotting $i/v^{1/2}$ as a function of $v^{1/2}$, allowing quantitative evaluation of the capacitive and diffusion-controlled charge-storage contributions at different scan rates (**Figure 4**).

Table S1. Molecular and Thermal Characteristics of Polyamides (**PQ-a** to **PQ-f**).

Polymer	Inherent Viscosity (dL/g)	Tg (°C)	Td @10% (°C, N_2)	Td @10% (°C, Air)	Structural Notes
PQ-a	0.80	232	454	473	Aliphatic diacid, flexible chain
PQ-b	0.54	254	474	466	Cycloaliphatic structure
PQ-c	0.28	338	497	491	Aromatic rigid backbone
PQ-d	0.96	250	538	523	Ether-containing aromatic
PQ-e	0.65	281	536	524	Sulfone-containing aromatic
PQ-f	0.62	293	531	494	CF_3-containing rigid backbone

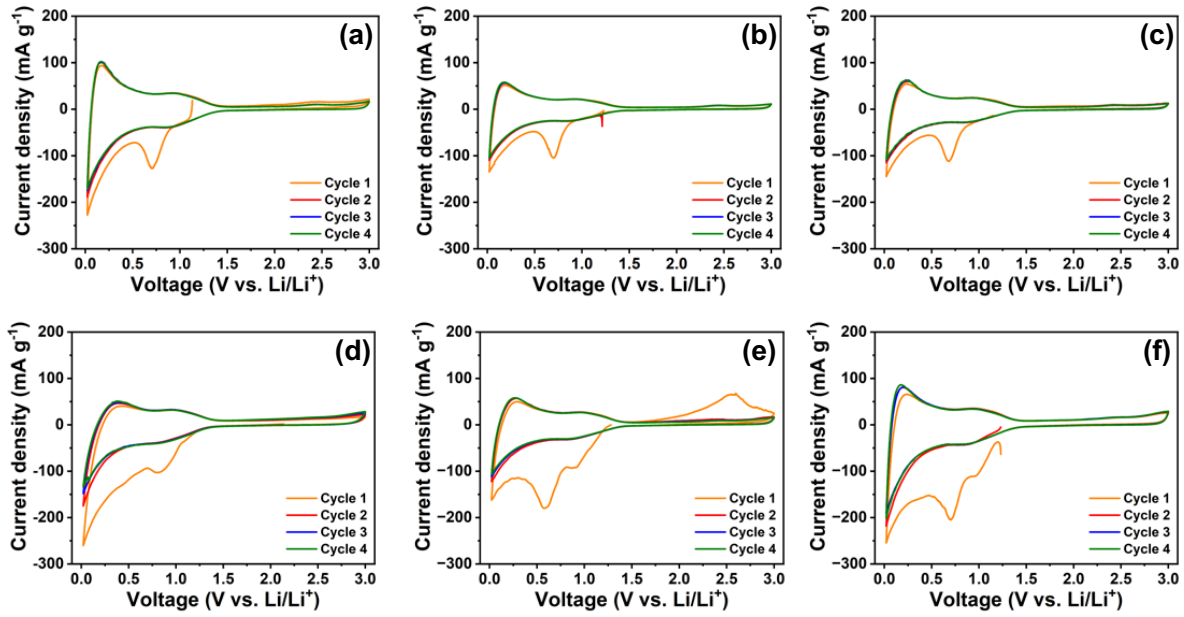

Figure S1. Cyclic voltammograms of (a) **PQ-a**, (b) **PQ-b**, (c) **PQ-c**, (d) **PQ-d**, (e) **PQ-e**, and (f) **PQ-f** recorded over the first four cycles at a scan rate of 0.1 mV s^{-1} in the voltage window of 0.02-3.0 V (vs. Li/Li^+), illustrating the evolution of redox behavior and stabilization of the lithiation-delithiation process upon initial cycling.

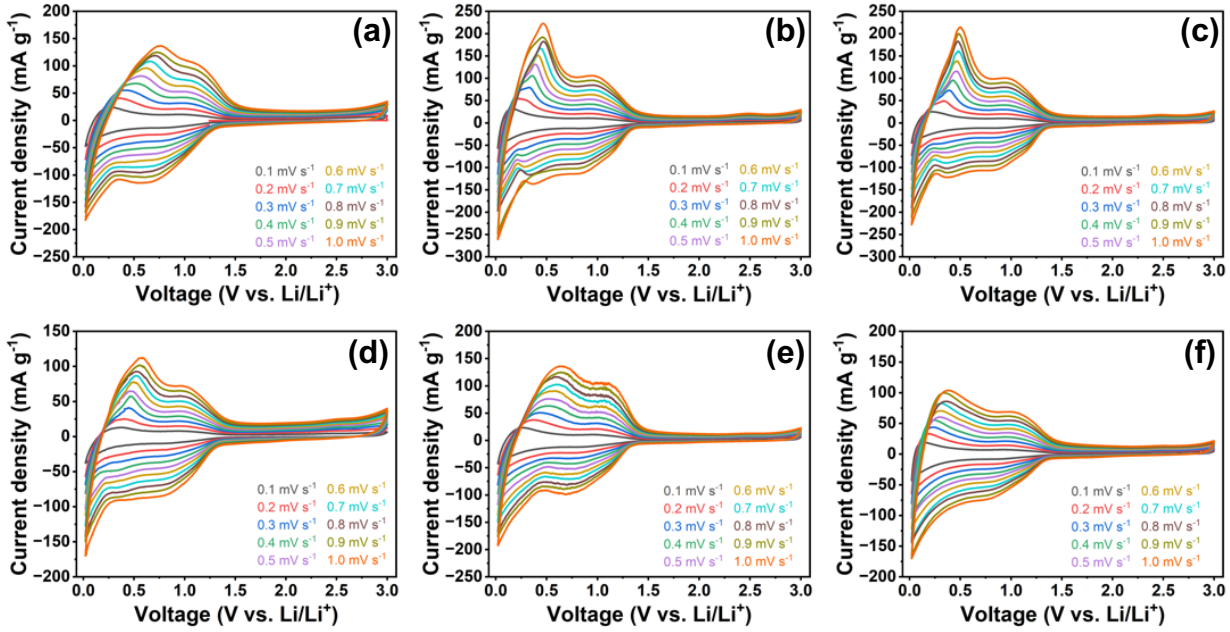

Figure S2. Cyclic voltammograms of a) **PQ-a**, (b) **PQ-b**, (c) **PQ-c**, (d) **PQ-d**, (e) **PQ-e**, and (f) **PQ-f** recorded at various scan rates ranging from 0.1 to 1.0 mV s^{-1} in the voltage window of 0.02-3.0 V (vs. Li/Li^+), illustrating the scan-rate-dependent redox behavior and kinetic characteristics of the polymer electrodes.

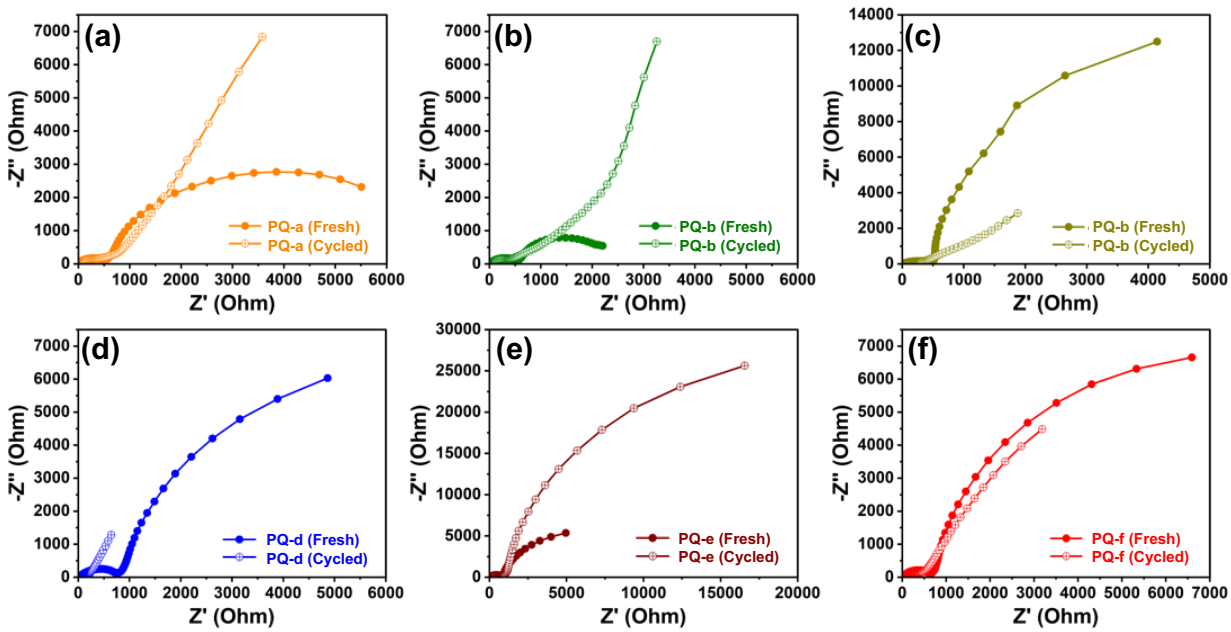

Figure S3. Nyquist plots of **PQ-polyamide** electrodes obtained from electrochemical impedance spectroscopy measurements (a) before cycling and (b) after cycling, showing the evolution of interfacial charge-transfer resistance and ion-transport behavior.

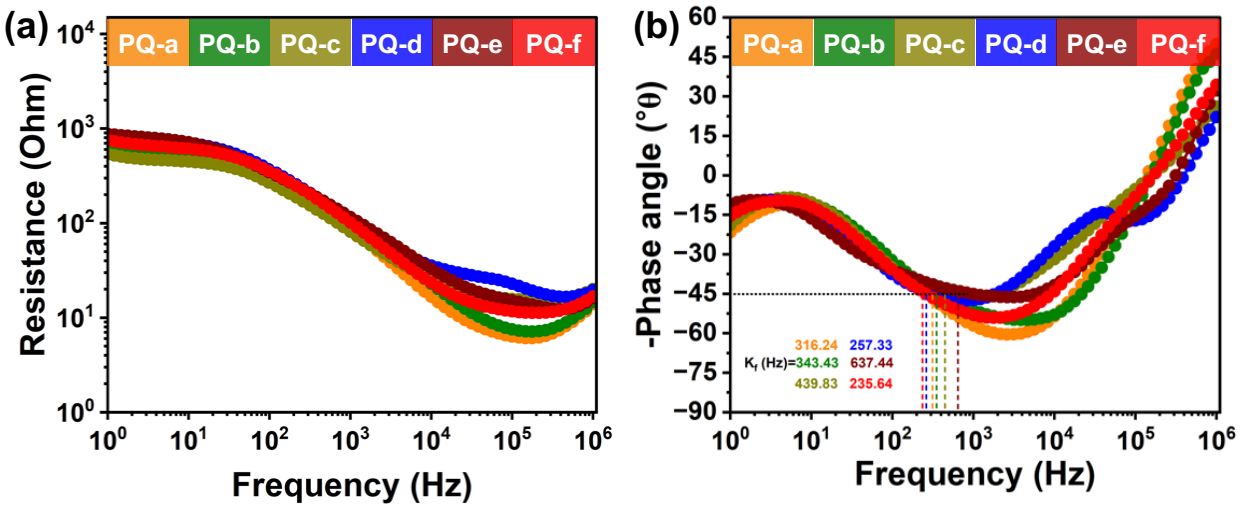

Figure S4. (a) Bode magnitude plots and (b) Bode phase plots derived from EIS spectra of **PQ-polyamide** electrodes. The knee frequency (f_k) and corresponding relaxation time constants (τ) extracted from the phase-angle minima are used to evaluate substituent-dependent electrochemical relaxation kinetics.

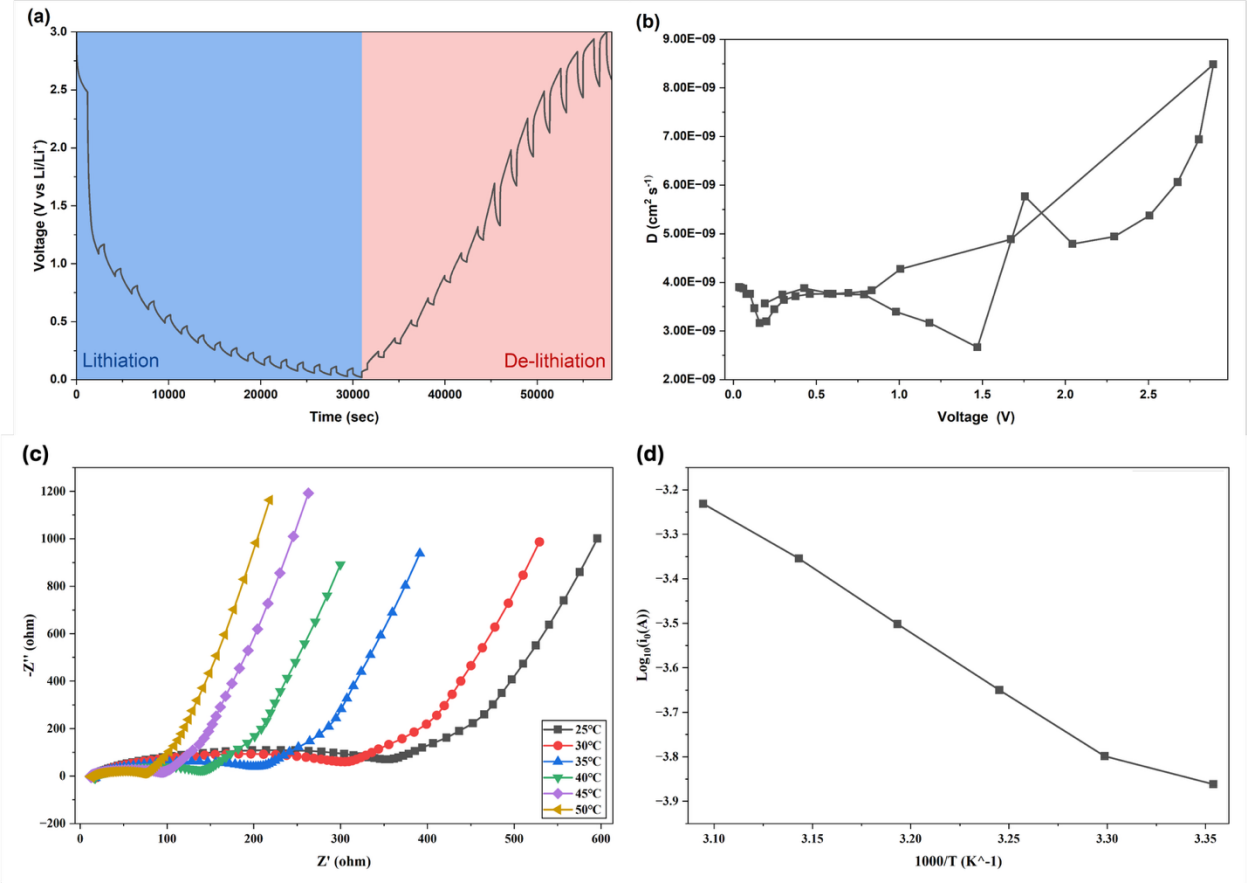

Figure S5. (a) GITT profile of **PQ-c** during lithiation and delithiation. (b) Lithium-ion diffusion coefficient (D_{li}^{+}) as a function of voltage derived from GITT. (c) Nyquist plots at different temperatures (25–50 °C). (d) Arrhenius plot of $\log_{10}(i_o)$ vs. 1000/T with an activation energy of 48.75 kJ mol^{-1}.

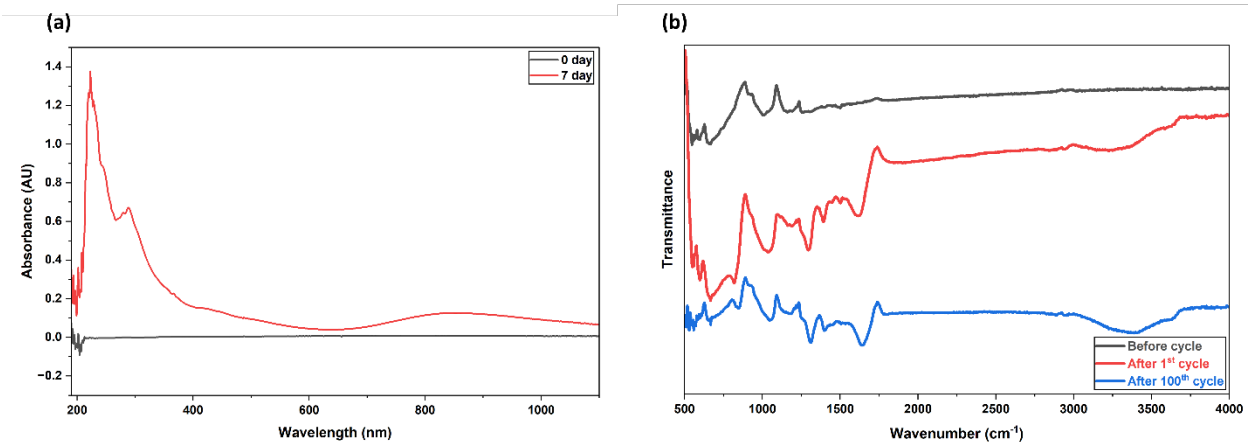

Figure S6. (a) Solubility tests, soaking **PQ-c** in 1 M $LiPF_6$ in EC:DEC (1:1 v/v) for 7 days, showing an increased absorbance after prolonged soaking, and (b) the ex-situ FTIR at three different statuses of **PQ-c** electrode.

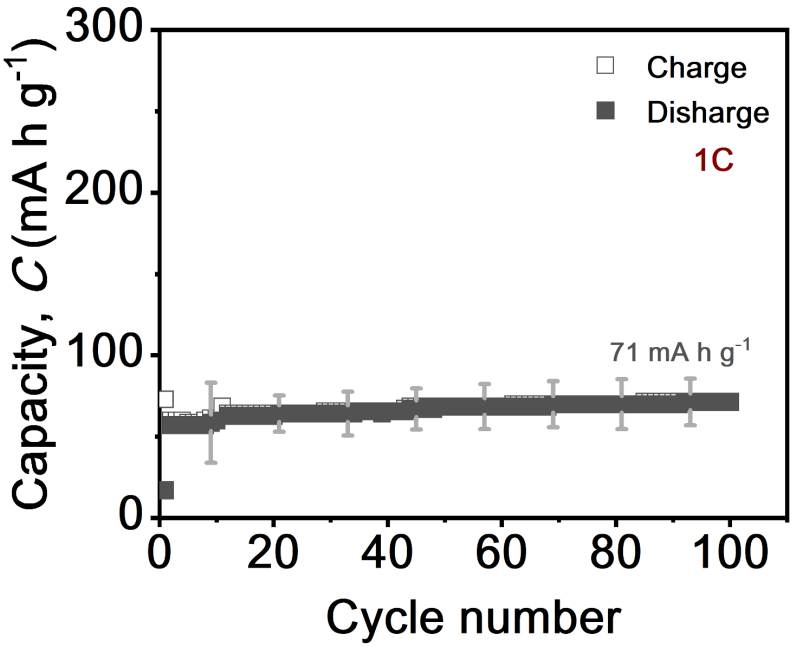

Figure S7. The electrochemical performance of a control electrode consisting of 90 wt.% Super P and 10 wt.% PVDF binder at 1C rate.

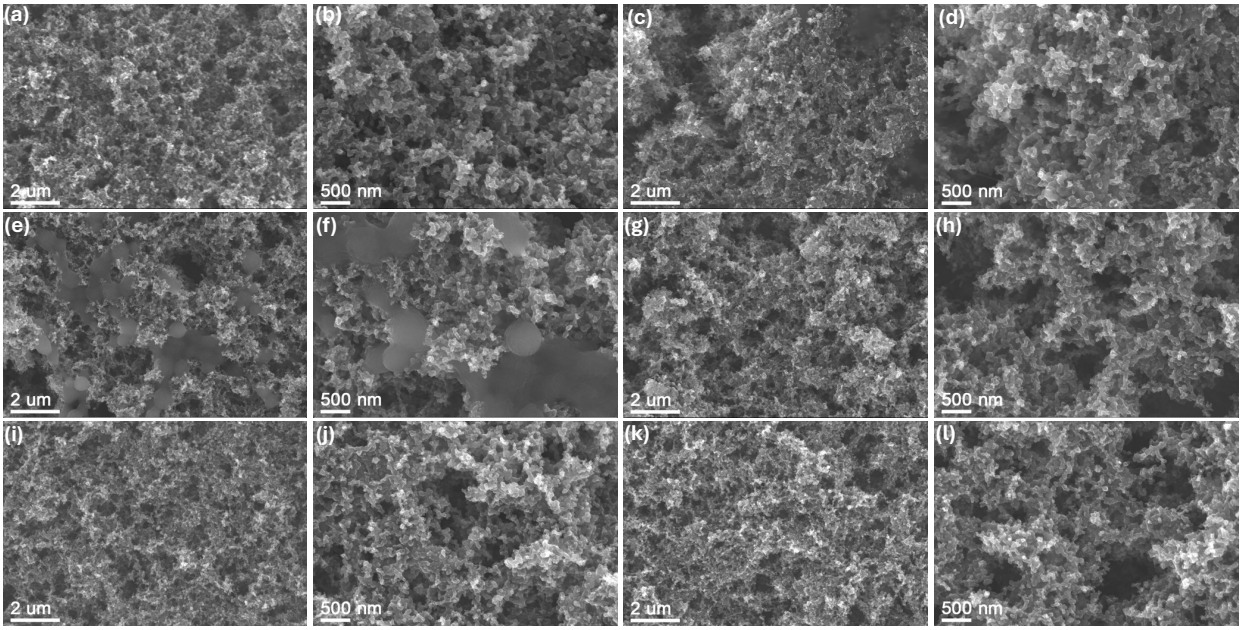

Figure S8. SEM images of **PQ-polyamides** at different magnifications (30k and 70k): (a–b) **PQ-a**, (c–d) **PQ-b**, (e–f) **PQ-c**, (g–h) **PQ-d**, (i–j) **PQ-e**, and (k–l) **PQ-f**.

Table S2. Summary of polymer based anodes for LIBs.

No.	Polymer	Voltage (V vs Li/Li^+)	Current density ($mA\ g^{-1}$)	Performance (Specific capacity($mAh\ g^{-1}$)/ cycle)	Ref.
1	Polydiaminophenylsulfone-triazine	0.0-3.0	100	565/100	8
			1000	375/100	
2	SNW-1/CNTs	0.01-3.0	500	203/1000	9
3	PI	0.001-3.0	100	578/50	10
4	PMAQ	0.01-3.0	500	465/150	11
5	N-CPIMs	0.0-3.0	10	500/5	12
6	PDCzBT	0.0-3.0	100	404/100	13
			200	312/400	
7	P(C-TDPP-TA)	0.01-3.0	100	357/500	14
	P(F-TDPP-TA)			298 /500	
	P(C-TDPP-H)			327 /500	
	P(F-TDPP-H)			278 /500	
8	P3-AQT	0.0-3.5	50	380/100	15
			100	400/100	
9	PTp-COOH	0.01-3.0	500	147/100	16
10	Poly(imine-anthraquinone) (PIAQ)	0.01-3.5	200	486/1000	***17***
11	Polyanthraquinone-triazine (PAT)	0.01-3.0	200	1770/400	18
12	Multi-carbonyl polyimide (PMTA)	0.01-3.0	100	698/50	19
13	BIAN-based porous organic polymer (PBM)	0.01-3.0	400	850/3000	20
			750	740/2000	
			1000	300/1100	
14	TTD-PDA	0.01-3.0	100	651/240	21
	TTD-EDA			492/400	
	GA-PDA Schiff-base polymer			416/300	
15	MA–VA–PcNi polymer	0.01-3.0	200	507/400	22
16	Itaconic acid–graphite composite anode	0.01-3.0	25	571/200	23
			100	693/200	
17	Tea-polyphenol–Ni chelate (TP-Ni) organic anode		100	454/500	24
18	**PQ-a**	**0.02-3.0**	**100**	**222/100**	**This work**
	PQ-b			**191/100**	
	PQ-c			**293/100**	
	PQ-d			**470/100**	
	PQ-e			**211/100**	
	PQ-f			**153/100**	

References.

1. J. Wang, J. Polleux, J. Lim and B. Dunn, *The Journal of Physical Chemistry C*, 2007, **111**, 14925–14931.
2. F.-F. Li, J.-F. Gao, Z.-H. He and L.-B. Kong, *ACS Applied Energy Materials*, 2020, **3**, 5448–5461.
3. V. Augustyn, J. Come, M. A. Lowe, J. W. Kim, P.-L. Taberna, S. H. Tolbert, H. D. Abruña, P. Simon and B. Dunn, *Nature materials*, 2013, **12**, 518–522.
4. F. Yu, Z. Liu, R. Zhou, D. Tan, H. Wang and F. Wang, *Materials Horizons*, 2018, **5**, 529–535.
5. H. Lindström, S. Södergren, A. Solbrand, H. Rensmo, J. Hjelm, A. Hagfeldt and S.-E. Lindquist, *The Journal of Physical Chemistry B*, 1997, **101**, 7717–7722.
6. T. C. Liu, W. Pell, B. Conway and S. Roberson, *Journal of the Electrochemical Society*, 1998, **145**, 1882.
7. F. Baskoro, H.-J. Lin, C.-W. Chang, C.-L. Wang, A. L. Lubis and H.-J. Yen, *Journal of Materials Chemistry A*, 2023, **11**, 569–578.
8. Q. Ma, J. Zheng, H. Kang, L. Zhang, Q. Zhang, H. Li, R. Wang, T. Zhou, Q. Chen and A. Liu, *ACS applied materials & interfaces*, 2021, **13**, 43002–43010.
9. S.-X. Xu, W. Xu, L.-J. Kong and Y.-H. Zhang, *SN Applied Sciences*, 2020, **2**, 199.
10. J. He, Y. Liao, Q. Hu, Z. Zeng, L. Yi, Y. Wang, H. Lu and M. Pan, *Ionics*, 2020, **26**, 3343–3350.
11. Z. Ba, Z. Wang, Y. Zhou, H. Li, J. Dong, Q. Zhang and X. Zhao, *ACS Applied Energy Materials*, 2021, **4**, 13161–13171.
12. X. Han, P. Han, J. Yao, S. Zhang, X. Cao, J. Xiong, J. Zhang and G. Cui, *Electrochimica Acta*, 2016, **196**, 603–610.
13. S. Zhang, W. Huang, P. Hu, C. Huang, C. Shang, C. Zhang, R. Yang and G. Cui, *Journal of Materials Chemistry A*, 2015, **3**, 1896–1901.
14. Z. Xu, S. Hou, Z. Zhu, P. Zhou, L. Xue, H. Lin, J. Zhou and S. Zhuo, *Nanoscale*, 2021, **13**, 2673–2684.
15. C. Zhang, S. Chen, G. Zhou, Q. Hou, S. Luo, Y. Wang, G. Shi and R. Zeng, *Journal of Electroanalytical Chemistry*, 2021, **895**, 115495.
16. H. Numazawa, K. Sato, H. Imai and Y. Oaki, *NPG Asia Materials*, 2018, **10**, 397–405.
17. Z. Man, P. Li, D. Zhou, R. Zang, S. Wang, P. Li, S. Liu, X. Li, Y. Wu and X. Liang, *Journal of Materials Chemistry A*, 2019, **7**, 2368–2375.
18. H. Kang, H. Liu, C. Li, L. Sun, C. Zhang, H. Gao, J. Yin, B. Yang, Y. You, K.-C. Jiang, H. Long and S. Xin, *ACS Applied Materials & Interfaces*, 2018, **10**, 37023–37030.
19. J. He, Y. Liao, Q. Hu, Z. Zeng, L. Yi, Y. Wang, H. Lu and M. Pan, *Journal of Power Sources*, 2020, **451**, 227792.
20. B. S. Mantripragada, R. Badam and N. Matsumi, *ACS Applied Energy Materials*, 2022, **5**, 6903–6912.
21. J. Zhang, X. Mu and Y. Mu, *ACS Omega*, 2024, **9**, 12967–12975.
22. J. Zhao, Y. Xu, J. Chen, L. Tao, C. Ou, W. Lv and S. Zhong, *Dalton Transactions*, 2021, **50**, 9858–9870.
23. R. Guo, Y. Wang, X. Shan, Y. Han, Z. Cao and H. Zheng, *Carbon*, 2019, **152**, 671–679.
24. Y. Guo, J. Guo, B. Li, Y. Zheng, W. Lei, J. Jiang, J. Xu, J. Shen, J. Li and H. Shao, *Inorganics*, 2023, **11**, 148.